


Cite this: *Nanoscale*, 2019, **11**, 11071

Latest progress in constructing solid-state Z scheme photocatalysts for water splitting

Xinyuan Xia,  ^{a*} Mengjiao Song, ^a Hua Wang, ^{b,c} Xiangtong Zhang, ^c Ning Sui, ^b Qingbo Zhang, ^d Vicki L. Colvin ^d and William W. Yu  ^{*b,c}

Artificial Z scheme photocatalysis has been considered as a promising strategy for producing the clean energy source of hydrogen gas. The core of the Z scheme is a two-step excitation process in a tandem structured photosystem aiming to satisfy both the criteria of wide range solar spectrum absorption and strong thermodynamic driving force for photolysis reactions. Therefore, efficient connection and matching between the two photosystems is the key to improve the photocatalytic activity. Recently, new progress has been achieved concerning the principles and applications of state-of-the-art solid-state Z schematic systems to enhance the photocatalytic efficiency and repress competitive reactions. This review summarizes the latest approaches to all-solid-state Z schemes for photocatalytic water splitting, including new tandem structures, new morphologies, and new connection modes to improve light absorption as well as carrier transportation. The challenges for developing novel high performance Z scheme photocatalysts are also discussed.

Received 15th April 2019,
Accepted 13th May 2019
DOI: 10.1039/c9nr03218e
rsc.li/nanoscale

1. Introduction

The growing need for more energy as well as the issues around environmental protection and climate change are among the

greatest challenges faced by humanity today. It is highly urgent to develop energy resources that are sustainable, clean and eco-friendly.¹ Solar energy is abundant, renewable and clean, and could meet the current and future global energy demand. However, it is still necessary to develop solar energy into a form that is easy to store, transport, and use. Among many possibilities, scalable hydrogen gas produced by solar energy induced water splitting is very promising.²

Since the Honda–Fujishima effect was discovered in 1972,³ semiconductor based photocatalysts for water splitting have become a hot topic. To catalyze the photolysis of water, the energy level of a semiconductor must meet the following

^aCollege of Chemistry, Chemical Engineering and Materials Science, Shandong Normal University, Jinan 250014, China. E-mail: voegleinne@163.com

^bCollege of Material Science and Engineering, Qingdao University of Science and Technology, Qingdao 266042, China. E-mail: wyu6000@gmail.com

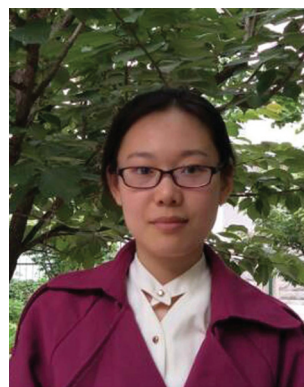
^cDepartment of Chemistry and Physics, Louisiana State University, Shreveport, LA 71115, USA

^dDepartment of Chemistry, Brown University, Providence, Rhode Island 02912, USA



Xinyuan Xia

Xinyuan Xia received his Ph.D. degree in inorganic chemistry at Peking University in 2012. He is now a lecturer in the College of Chemistry, Chemical Engineering and Materials Science at Shandong Normal University. His research mainly focuses on photocatalytic water splitting, CO₂ reduction, and N₂ fixation by earth-abundant materials.



Mengjiao Song

Mengjiao Song received her BS degree in chemistry from Qufu Normal University in 2016. She is currently working on her MS degree at Shandong Normal University under the supervision of Dr Xinyuan Xia. Her research focuses on photocatalytic water splitting by non-noble metal compounds.

requirements. (1) The bandgap must be larger than 1.23 eV to meet the minimum dynamic requirement of water decomposition into H_2 and O_2 . (2) The conduction band should be more negative than the reduction potential of H^+/H_2 (0 V vs. RHE) and the valence band should be more positive than the oxidation potential of $\text{O}_2/\text{H}_2\text{O}$ (1.23 V vs. RHE).⁴ In practice, because of the existence of overpotentials for the hydrogen and oxygen evolution half reactions, the bandgap should be more than 1.8 eV, which means that the semiconductor cannot use near-infrared light (>750 nm), which accounts for more than 40% of the total sunlight energy.⁵ It is difficult for single semiconductor catalyzed water splitting to satisfy both the criteria of wide range solar spectrum absorption and strong thermodynamic driving force for photolysis reactions. Additionally, to date, only a few semiconductors can achieve “overall water splitting” (realizing both hydrogen and oxygen evolution in the conduction and valence bands, respectively^{4,6–8}). Most reported semiconductors for “water splitting” can only achieve one of the two half-reactions, which necessitates the assistance of sacrificial agents to suppress charge accumulation and carrier recombination.

Inspired by the natural photosynthesis in plants (Fig. 1A), single semiconductor photocatalysis (Fig. 1B) has been replaced by artificial photocatalytic systems (Fig. 1C) with two combined semiconductors, which have been developed in the last two decades.⁹ The core of this system is a two-step excitation process in a tandem structure: photosystem I (PS I) and photosystem II (PS II) are both excited by incident light. The photogenerated electrons in the conduction band (CB) of PS I and holes in the valence band (VB) of PS II accomplish the reduction reaction and oxidation reaction with water or sacrificial agents, respectively. The charge transfer path resembles a “Z” shape in terms of energy levels, hence the name “Z scheme system”.^{10–13} In the last two decades, numerous research efforts have been made to design and synthesize Z schematic photocatalysts for various applications including water splitting, CO_2 conversion, and chemical photodegradation, which have been introduced in several review articles.^{89,90} In contrast to single semiconductor photocatalysis, the Z

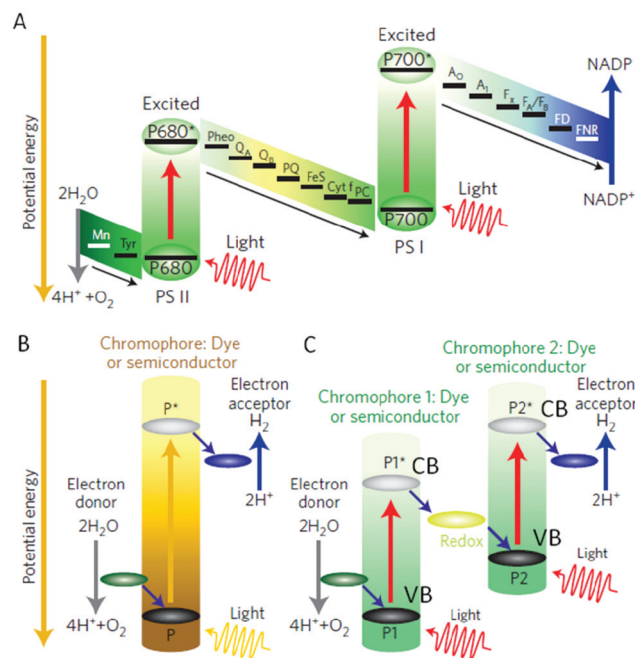


Fig. 1 Scheme of (A) natural, (B) single conductor, and (C) artificial Z scheme photosynthesis. Mn = manganese calcium oxide cluster, Tyr = tyrosine in PS II, Pheo = pheophytin, the primary electron acceptor of PS II, QA = primary plastoquinone electron acceptor, QB = secondary plastoquinone electron acceptor, PQ = plastoquinone, FeS = Rieske iron sulphur protein, Cyt. F = cytochrome f, PC = plastocyanin, A0 = primary electron acceptor of PS I, A1 = phyloquinone, FX, FA, FB = three separate iron sulphur centres, Fd = ferredoxin, FNR = nicotinamide adenine dinucleotide phosphate (NADP) reductase. Reproduced from ref. 9 with permission. Copyright 2012 Nature Publishing Group.

scheme system is no longer limited by the strict demands of thermodynamics and the overpotential for water decomposition, resulting in a wider range of material choices, as any two narrow-bandgap semiconductors with appropriate CB and VB levels can be integrated into an efficient water splitting photocatalyst. Although the Z scheme system theoretically needs to absorb more photons than a single photocatalyst to split the same amount of water, the absorption range of the two semiconductors can be adjusted to be complementary to each other. It is thus clear that artificial Z scheme systems are designed to provide an efficient combination of two semiconductor photocatalysts with broad solar light utilization and strong redox ability while not necessarily suppressing the theoretical apparent quantum efficiency.

For the main reaction of photocatalytic water splitting in an artificial Z scheme system, the photogenerated electrons in the CB of PS II and photogenerated holes in the VB of PS I should recombine to connect the reduction/oxidation reactions with water. This is the key step for the Z schematic charge flows and often requires an “electron mediator” to afford sites for carrier recombination and relay. Notably, the Z schematic mechanism implies the emergence of non-negligible backward reactions accompanying water splitting. Therefore, an important challenge is to develop suitable electron mediators for PS I and PS



William Yu

William Yu obtained his PhD degree from the Institute of Chemistry, Chinese Academy of Sciences. His research interests are solution dispersible nano-materials and their applications in alternative energy, biomedicine, and environmental remediation.

II in order to realize efficient coupling of electrons and holes with weak redox ability and promote the water photolysis reaction while making the competitive reactions thermodynamically unfavorable. Through years of effort, a large group of acceptor/donor (A/D) pairs of soluble ions (shuttle redox mediators) have been developed for Z schemes to relay the charge carriers from one photosystem to the other ($\text{Fe}^{2+}/\text{Fe}^{3+}$, I^-/I^{3-} , I^-/IO_3^- , etc.).^{14–18} The electron donor consumes holes in the VB of PS I and the acceptor consumes electrons in the CB of PS II. However, the low diffusion rates of ions in liquid media limit the charge carrier transfer. Additionally, the soluble redox shuttles may compete with water splitting by reacting with the charges that are intended to produce hydrogen/oxygen gases. These drawbacks of soluble mediators necessitate the discovery of all-solid-state Z schemes with insoluble electron mediators that directly link PS I and PS II.^{19,20}

This review focuses on the latest developments in all-solid-state Z schemes for photocatalytic water splitting. The crucial factors of catalytic performance (morphology, structure, material choice, and interface) will be discussed and a number of significant issues and challenges will be highlighted. Notably, these PS I/mediator/PS II solid composite structures form at least two junctions between shuttle and photosystems, making it difficult to evaluate the photocatalytic performance before completing the process of catalyst synthesis.²¹ The aforementioned solid mediators thus should meet four crucial requirements: high intrinsic conductivity, reduced energy barriers for the junctions between PS I/mediator/PS II for minimized interfacial contact resistance, high stability during the photocatalytic process, and reduced shielding effect to suppress the light absorption by the mediator itself.

2. Z schemes with solid mediators

2.1 Suspended composite particles

In an all-solid-state Z scheme system, the PS I and PS II particles should above all have close contact with the solid mediator so that photogenerated charges can smoothly migrate and recombine at the mediator surface. Thus, a suspended solution of composite particles with the structure PS I/mediator/PS II is most commonly chosen for research into Z schemes. In this composite particle structure, it is considered that the CB of PS II and VB of PS I should achieve an ohmic contact rather than a Schottky barrier through the solid mediator to reduce the resistance to the migration of electrons and holes.²² Since noble metals (Au, Ag, Ir, etc.) combine the advantages of high work function and good stability in solution with an inherent photocorrosion-resistant nature, they have been the most commonly reported metal electronic mediators.^{23–27} The first solid state Z scheme system was reported by Tada *et al.* for methyl viologen reduction²⁸ by synthesizing a $\text{Au}@\text{CdS}/\text{TiO}_2$ photocatalyst with core-shell structure in which CdS, TiO_2 , and Au nanoparticles acted as the PS I, PS II and electron mediator, respectively. This composite catalyst accomplished a significantly enhanced photo-

catalytic activity, which originated from the Z scheme charge flow. This work paved the way to construct similar solid state Z scheme systems.^{24,29}

Plenty of studies have been done on Au based solid Z schemes in the last few years. Wang *et al.* connected the plasmonic photocatalyst Au/TiO_2 , which has oxygen evolution activity, with $\text{SrTiO}_3:\text{Rh}$ to achieve overall water splitting.³⁰ The maximum change in surface potential induced by simultaneous excitation of surface plasmon resonance (SPR) and $\text{SrTiO}_3:\text{Rh}$ revealed that Au acted not only as a charge transfer bridge but also as a photo-absorber owing to the SPR effect. A similar approach was reported by Zou *et al.*³¹ In their work, $\text{g-C}_3\text{N}_4/\text{Au}/\text{C-TiO}_2$ hollow spheres were formed. UV/Vis DRS spectra showed that the SPR effects of Au facilitated visible light absorption and energy utilization. As a result, the Z scheme catalyst improved hydrogen production by a factor of 86 and 42 compared to pure C-TiO_2 and $\text{g-C}_3\text{N}_4$. Notably, a Z scheme system of $\text{WO}_3/\text{Au}/\text{In}_2\text{S}_3$ fabricated by Li *et al.* displayed evidence of Z schematic charge flow according to measurements of the surface potential change using Kelvin probe force microscopy. The holes were revealed to migrate from In_2S_3 to WO_3 through the Au mediator when In_2S_3 and WO_3 were both excited by incident light, resulting in enhanced charge separation and prolonged carrier survival time, and significantly improved photocatalytic activity.⁹¹

However, noble metals (Au, Pt) inevitably face a severe challenge as electron mediators because they have good catalytic properties for the reverse process of water oxidation (oxygen reduction reaction, ORR), a competitive reaction which can significantly reduce the quantum efficiency of photocatalytic water splitting.³² Recently, it was found that ORR could be successfully inhibited *via* protection by Cr_2O_3 , amorphous TiO_2 , or oxyhydroxides of Ti, Nb, and Ta layers.^{33–36} Additionally, Ag is also a candidate to act as a solid mediator in Z scheme water splitting systems. Kobayashi *et al.* reported a $\text{ZnRh}_2\text{O}_4/\text{Ag}/\text{Ag}_{1-x}\text{SbO}_{3-y}$ catalyst,²⁵ in which the nanosized Ag particles offered more surface area and active sites for charge recombination. $\text{Ir}/\text{CoO}_x/\text{Ta}_3\text{N}_5$ was combined with $\text{SrTiO}_3:\text{La}/\text{Rh}$, in which Ir functioned as a solid mediator to obtain a 3.8 times higher activity for water splitting.³⁷ Additionally, some transition metals were recently demonstrated as effective charge transfer mediators, such as W in $\text{WO}_3/\text{W}/\text{PbBi}_2\text{Nb}_{1.9}\text{Ti}_{0.1}\text{O}_9$ and Cd in $\text{ZnO}/\text{Cd}/\text{CdS}$.^{38,39} The aforementioned conductive metals also provided active sites for photoinduced charge transfer and recombination.

Although, to some extent, the catalytic activity of noble metals for ORR can be suppressed by protection layers, the backward reaction still takes place at ambient conditions, which has negative influences on catalytic water splitting.⁴⁰ In the past few years, another emerging solid-state electron mediator is carbonaceous materials, represented by reduced graphene oxide (RGO)^{41–43} and carbon dots (CDs).^{44,45} The large surface area, good conductivity and tunable bandgaps of RGO afford plenty of pathways and sites for Z scheme charge flow and recombination.⁴⁶ The semiconductors of PS I and PS II can be connected to RGO by electrostatic adsorption or

chemical bonding. Moreover, RGO is less expensive than noble metals, and non-doped RGO is catalytically inert to competitive ORR. Iwase *et al.* reported that photoreduced graphene oxide (PRGO) could act as an efficient solid shuttle to transport photogenerated electrons in PS II (BiVO_4) and holes in PS I ($\text{Ru/SrTiO}_3\text{:Rh}$) in order to accomplish an overall water photolysis reaction under visible light.¹⁹

The key factor to success in high performance water splitting is the balance of conductivity and hydrophobicity of RGO. Well reduced RGO (*e.g.* by hydrazine) has good conductivity for electron flow but easily aggregates in water due to the hydrophobic nature of C—C bonds. Either hydrazine-reduced GO or photo-reduced GO by $\text{Ru/SrTiO}_3\text{:Rh}$ failed to achieve a higher catalytic activity because they were over reduced so that the catalyst particles were not miscible in water. In contrast, GO photoreduced by BiVO_4 contained an appropriate amount of C—O bonds which led to a good dispersion in aqueous solution, revealing the importance of rational control of the degree of reduction of GO as an electron mediator. Kudo and co-workers coupled a series of p-type metal sulfides to an RGO-n-type PS II (TiO_2 , BiVO_4) for water photolysis and CO_2 reduction.^{47,48} The combinations of different PS I and PS II resulted in quite different photocatalytic performances. The overlapped potential area of photocurrent between the photoelectrodes made by the PS I and PS II counterparts was crucial for the improvement of the water splitting behavior.⁴⁷ It is widely considered that the morphology of catalysts is of great importance for the photocatalytic activity. Liu *et al.* made a $\text{CeVO}_4/3\text{D RGO aerogel/BiVO}_4$ ternary catalyst.⁴¹ The unique 3D structure of RGO afforded not only abundant surfaces for contact between PS I and PS II nanoparticles, but also an interconnected network of bridges for fast charge migration, leading to an improvement of O_2 evolution by a factor of 2.1 in contrast to bare BiVO_4 .

CDs are another promising group of cost effective 0D nanomaterials with long-term stability and good photogenerated charge transfer properties. CDs act as a unique component of high performance photocatalysts and photoelectrocatalysts.^{49–52} Particularly, CDs have a great potential to be an ideal solid mediator in Z scheme systems. Using BiVO_4 and CdS nanoparticles acting as PS II and PS I, respectively, Kang and co-workers coupled them with a CD mediator to construct a $\text{BiVO}_4/\text{CD}/\text{CdS}$ Z scheme system for pure water splitting.⁴⁴ Because CDs can perform as either electron donors or acceptors with high quenching efficiency,^{53,54} photoinduced electrons and holes easily transfer to the surface of CDs, extending the lifetime of the charges for H_2 and O_2 evolution. As a result, both catalytic behavior and reaction stability are significantly enhanced. Liu *et al.* developed another solid state Z scheme photocatalyst, $\text{NiO}/\text{CD}/\text{BiVO}_4$.⁴⁵ For overall water photolysis, the introduction of CDs enhanced the H_2 and O_2 evolution rates and raised the apparent quantum efficiency (AQE) to 1.24% under 420 nm light.

2.2 Particulate sheet photocatalysts

For most all-solid-state Z scheme photocatalysts, the key factor for enhancing catalytic activity is the photoinduced interparti-

cle electron and hole transfer. The rate determining step is charge migration between PS I and PS II through solid mediators. Aiming to address this challenge, Domen and co-workers designed a special Z scheme structure in which PS I and PS II particles were immobilized in a conductive sheet to form a particulate thin layer. The conductive sheet served as solid mediator in intimate contact with both the fixed PS I and PS II particles. This structure significantly facilitated charge transfer through the continuous-phase mediator to reduce the resistance and promote both HER and OER on the photocatalysts.^{23,32,55,56}

In the particulate sheet photocatalyst of $\text{SrTiO}_3\text{:La,Rh}/\text{Au layer}/\text{BiVO}_4\text{:Mo}$, the PS I and PS II nanoparticles were embedded closely in the Au mediator sheets.³² With careful control of the annealing time and temperature, a much lower contact resistance to charge transfer was obtained and the Schottky barrier between the Au layer and semiconductor photocatalysts was reduced. As a result, this photocatalyst achieved a dramatically high STH (solar-to-hydrogen) efficiency of 1.1% under 419 nm light. Aiming for large scale and fast production of catalysts, the authors also integrated the PS II and PS I photocatalysts with Au nanoparticles into a colloidal ink and screen printed it on a sheet.³² Although the screen printed sheets-based catalyst had an STH of only 0.1% and impaired long term stability due to the poorly controlled co-catalyst thickness and aggregation of Au, this method has a great potential for facile production of catalysts. A similar Z scheme catalyst using an Au layer as mediator was reported by Pan *et al.* $\text{RhCrO}_x/\text{LaMg}_{1/3}\text{Ta}_{2/3}\text{O}_2\text{N}$ and rutile- TiO_2 functioned as PS I and PS II, respectively. The two components were embedded in the Au layer capped by an amorphous TiO_2 protective layer. Under UV light irradiation, this catalyst realized overall water splitting into H_2 and O_2 .³⁶

In order to further suppress the backward reaction caused by the Au layer, conductive carbon sheets have also been selected as charge transport connectors in Z scheme systems. Wang *et al.* developed a $\text{SrTiO}_3\text{:La,Rh}/\text{C}/\text{BiVO}_4\text{:Mo}$ photocatalyst to split pure water without the assistance of shuttle ions, sacrificial reagents and buffering solutions⁴⁰ (Fig. 2). The work function of carbon (5.0 eV) was reported to be similar to those of Au (5.1 eV) and Rh (5.0 eV),^{57,58} making it suitable for recombining photogenerated electrons and holes from the CB of $\text{BiVO}_4\text{:Mo}$ and VB of $\text{SrTiO}_3\text{:La,Rh}$, respectively. Carbon layers are commonly used as a supporting substrate for ORR electrocatalysts. Their inactivity for ORR compared to Au significantly suppressed the backward reaction in Wang *et al.*'s system. The catalyst achieved an STH of 1.2% at 331 K and 10 kPa, and the STH remained as high as 1.0% even at 91 kPa. Both of these results are among the top performances for Z schematic pure water splitting. Moreover, the overpotentials of HER and OER and the resistance between the PS I and PS II were observably reduced, and the use of cost-effective carbon sheets instead of noble metals boosts the scalable and facile production of novel Z scheme catalysts for water photolysis.

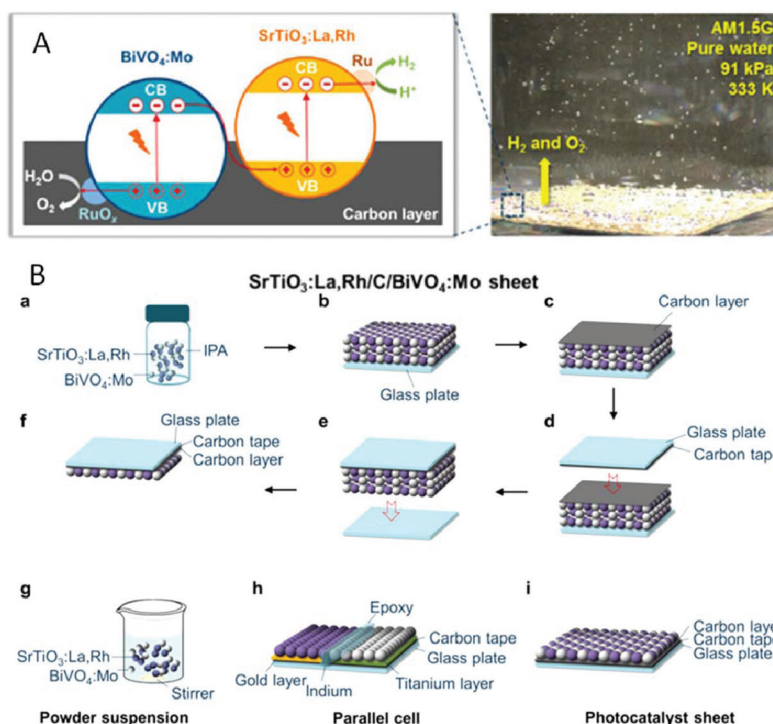


Fig. 2 (A) Schematic illustration of $\text{SrTiO}_3:\text{La,Rh}/\text{C}/\text{BiVO}_4:\text{Mo}$ photocatalyst sheet. (B) Scheme of the preparation process for the photocatalyst sheet by particle transfer. Reproduced from ref. 40 with permission. Copyright 2017 American Chemical Society.

Noble metals and carbonaceous materials suffer from shielding effects due to their significant absorption in the visible and near-infrared region. In this context, it is worth noting that transparent metal oxides may have tremendous potential in constructing novel Z scheme catalysts to solve this problem. Wang *et al.* demonstrated that nanoparticulate (np) indium tin oxide (ITO) can be applied as a transparent mediator to connect $\text{SrTiO}_3:\text{La,Rh}$ and $\text{BiVO}_4:\text{Mo}$ modified with Ru and Cr_2O_3 , respectively⁵⁹ (Fig. 3). The photocatalyst sheets had an STH of 0.4%, higher than most Z scheme catalysts using the same PS I and PS II and Au nanoparticle mediators, due to the high transparency of ITO to visible light and its inactivity to ORR. Furthermore, this catalyst sheet was fabricated by facile screen-printing with no vacuum procedures. This work highlighted that the appropriate choice of sophisticated materials promoted the application of transparent conductive mediators in low cost and fast fabrication of photocatalyst sheets for inexpensive and scalable solar fuel production.

3. Direct Z scheme systems

For all-solid-state Z scheme systems, owing to their similar band structures to a type-II heterojunction, it is crucial to manipulate the built-in electric field in PS I and PS II in order to ensure a Z schematic mode for the flow of photogenerated electrons and holes rather than an inverse mode as in a type-II heterojunction. Thus, solid (particles, sheets, *etc.*) metallic

and carbonaceous mediators are inserted into PS I and PS II semiconductors to form a ternary Z scheme photocatalyst. However, solid mediators have non-negligible drawbacks such as backward reactions, shielding effects and photocorrosion, which limit the activity and stability of the catalyst. Very recently, a kind of photocatalyst known as the direct Z scheme has emerged as a hotly tipped candidate for water splitting. In these photocatalysts, solid mediators are removed and PS I and PS II are integrated directly into a simple binary structure *via* intimate contacts, and the photogenerated electrons in the CB of PS II and holes in the VB of PS I recombine at the interface of the two semiconductors.^{14,60} This simple structure of a direct Z scheme without independent mediators has several advantages. First, the temporal stability of the direct Z scheme is considerably prolonged because of the resistance to photocorrosion.⁶¹ Second, backward reactions are substantially weakened. Third, the shielding effect is significantly reduced. Finally, compared to the traditional ternary Z scheme, the binary structure of the direct Z scheme is more favorable to facile and cost-effective fabrication of photocatalysts.

In order to successfully establish a direct Z scheme system, the combination of PS I and PS II is the key consideration, which relates to the amount and architecture of the two semiconductors and the morphology and electronic structure of the interface between PS I and PS II. For example, a $\text{g-C}_3\text{N}_4/\text{CdS}$ heterostructure demonstrated different types of electron flows depending on different synthesis routes (Fig. 4). When CdS was photodeposited on $\text{g-C}_3\text{N}_4$, it tended to grow at the electron transfer sites of $\text{g-C}_3\text{N}_4$, resulting in a type-II heterojunc-

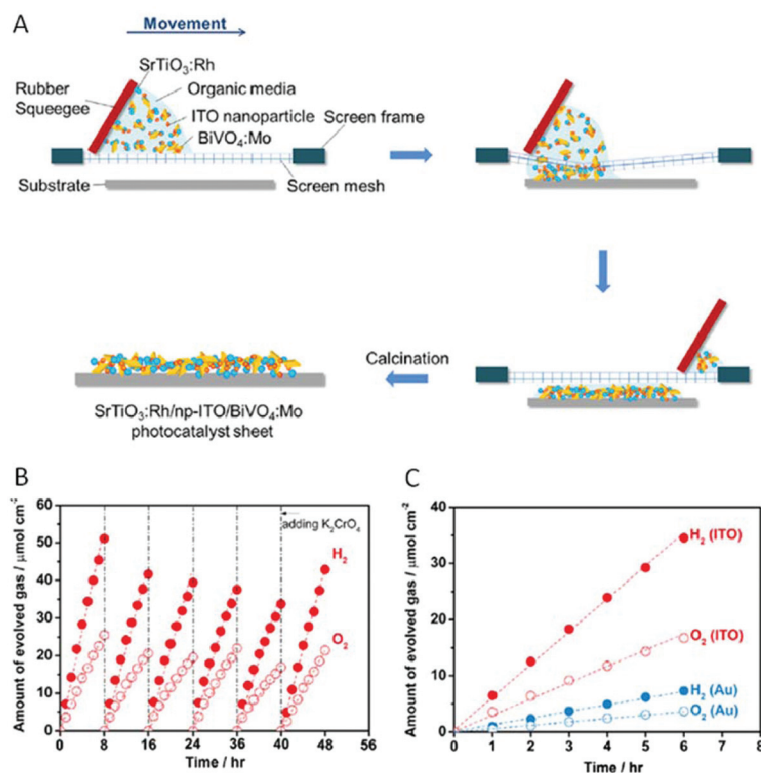


Fig. 3 (A) Scheme of the preparation of a SrTiO₃:Rh/np-ITO/BiVO₄:Mo sheet by screen printing. (B) Photocatalytic H₂ and O₂ evolution on a Cr₂O₃/Ru co-loaded SrTiO₃:Rh/np-ITO/BiVO₄:Mo photocatalyst sheet. (C) Photocatalytic H₂ and O₂ evolution on Cr₂O₃/Ru co-loaded SrTiO₃:La,Rh/np-ITO/BiVO₄:Mo (red) and SrTiO₃:La,Rh/np-Au/BiVO₄:Mo sheets (blue) under simulated sunlight (AM 1.5G) at 333 K and 91 kPa. Reproduced from ref. 59 with permission. Copyright 2018 Elsevier.

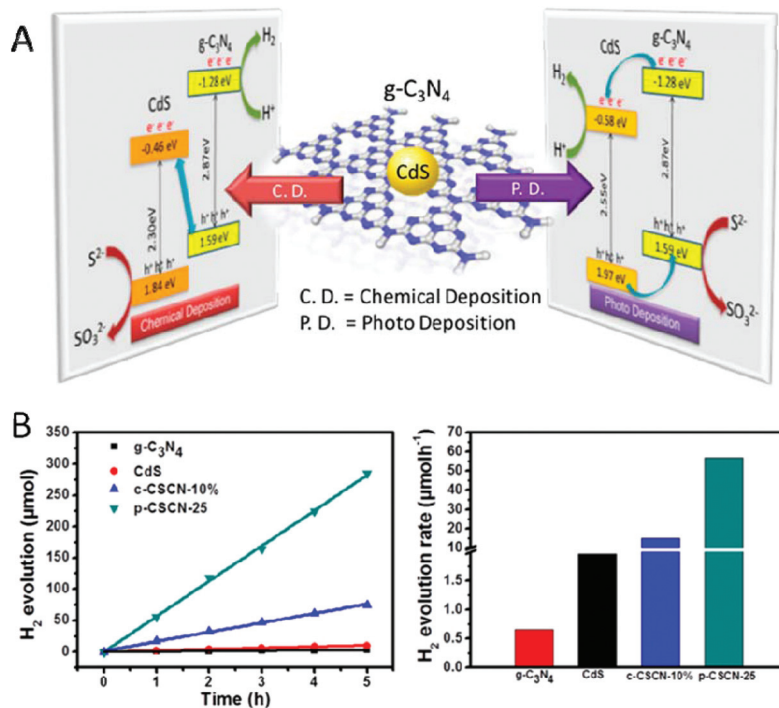


Fig. 4 (A) Schematic illustration of different types of g-C₃N₄/CdS heterostructures depending on synthesis methods. (B) Photocatalytic H₂ evolution rates of the composite photocatalysts. Reproduced from ref. 62 with permission. Copyright 2018 American Chemical Society.

tion of g-C₃N₄/CdS. However, when CdS was chemically deposited *via* the hydrothermal method, there was little selectivity of deposition sites, leading to a direct Z schematic electron flow from the CB of g-C₃N₄ to the VB of CdS.⁶² Although chemically deposited g-C₃N₄/CdS has a lower H₂ production activity than that of the photodeposited system, this work indicates the importance of rational design and synthesis route selection for regulation of direct Z scheme systems.

It is noteworthy that due to the requirement of fast interfacial charge transfer, an intimate contact between PS I and PS II is preferred. Particularly, chemical bonds can promote interfacial connections between semiconductors. Yu and coworkers found that the covalent W–O–N–(C)₂ significantly favored charge migration from WO₃ to g-C₃N₄ to form an efficient direct Z scheme.⁶³ In another work, CoTiO₃ microrods and g-C₃N₄ nanosheets were integrated into a unique 1D/2D structured CoTiO₃/g-C₃N₄ Z scheme catalyst.⁶⁴ It was found that the formation of Co–O–N or Ti–O–N bonds gave rise to an intimately combined CoTiO₃–g-C₃N₄ interface to achieve a high H₂ evolution rate of 858 μmol h^{−1} g^{−1}. Furthermore, chemical bonding can help to introduce new components into a direct Z scheme that dramatically improve the photocatalytic performance. An ultrathin In₂O₃–ZnIn₂Se₄ (In₂O₃–ZiSe) sheet was reported by Guo and coworkers.⁶⁵ In this work, Mo atoms were doped into an In₂O₃–ZiSe Z scheme by a solvothermal reaction and connected with Se to form Mo–Se bonds. Because MoSe₂ served as a co-catalyst for HER, the In₂O₃–ZiSe–Mo photocatalyst exhibited a 21.7 times higher efficiency in H₂ evolution than the non-doped In₂O₃–ZiSe system.

Another crucial factor for direct Z schemes with superior activity is the recombination interface for the photogenerated electrons in the CB of PS II and holes in the VB of PS I. Hence, there has been much discussion on the role of defects at the interface of PS I and PS II. Generally, crystalline semiconductors with minimal defects are beneficial to boost the interfacial charge transfer. Nevertheless, it has been revealed that surface defects play the role of trapping sites for electron–hole recombination by forming a series of intermediate energy levels in the semiconductor bandgaps, which enables the interface of PS I and PS II to achieve approximately ohmic contact.⁶⁶ Xing *et al.* fabricated boron/carbon nitride (BCN)–TiO_{2–x} using carbon doped hexagonal boron nitride (BN) and TiO₂ with surface oxygen vacancies.⁶⁷ Steady-state and time-resolved photoluminescence spectra displayed that the charge separation efficiency was enhanced and charge lifetime was prolonged. Namely, charges with strong redox ability were stabilized, which meant that charges with weak redox ability in the direct Z scheme successfully recombined at the good interface between TiO_{2–x} and BCN due to the existence of surface oxygen vacancies on TiO₂. For metal containing semiconductors, the improved charge recombination at defective interfaces is attributed to the presence of partial valence states of metal cations induced by surface defects and vacancies. Mo *et al.* hydrothermally synthesized a MnO₂/monolayer g-C₃N₄ Z scheme catalyst with partial defects of Mn³⁺.⁶⁸ The Mn³⁺ defects underwent a redox cycle between Mn³⁺ and Mn⁴⁺ to

serve as active sites for Z scheme interfacial charge transfer. As a result, the photocatalyst achieved a superior external quantum efficiency (EQE) of 23.33% under 420 nm light for hydrogen evolution, which was among the top values reported for g-C₃N₄-based photocatalysts. Recently, a dual defective Z scheme photocatalyst was synthesized by Gao *et al.*⁶⁹ in which the coupled PS I (g-C₃N₄ nanosheets) and PS II (TiO₂) were both defect enriched. Due to the narrowed bandgaps and additional reactive sites afforded by the dual defects, the photocatalyst had a dramatically high H₂ production activity of 651.79 μmol h^{−1} and a turnover frequency (TOF) of 419.3 h^{−1}, which remains the benchmark for defective TiO₂ or g-C₃N₄ based photocatalysts to date. This work highlighted the non-negligible importance of surface defects in direct Z scheme systems.

On the other hand, in the process of introducing defects on the semiconductor surface, it is difficult to control the regional selectivity of the defect distribution. That is, defects may appear not only at the interface between PS I and PS II, but also at the interface between the semiconductors and the external solution containing the reactants. In consequence, these defects at the solid–liquid interface may act as charge trapping centers so that the electrons and holes with strong redox ability may prefer to recombine on the surface rather than participate in water photolysis. Based on this consideration, the delicate balance of the “inner interface” for charges with weak redox ability and “outer interface” for charges with strong redox ability is decisive for Z schematic water splitting, indicating that the behavior of the photocatalyst is highly morphology dependent. The architecture and stoichiometric ratio of PS I and PS II thus play a critical role in enhancing the performance of Z scheme systems.

A heterostructure of MoS₂ quantum dots (QDs)/g-C₃N₄ with 0D/2D geometry was hydrothermally synthesized.⁷¹ The quantum confinement effect of the MoS₂ QDs accelerated charge transfer and reduced charge recombination by lowering the overpotential and resistance. Furthermore, the small MoS₂ QDs successfully formed a Z schematic mechanism with g-C₃N₄ due to their matched energy levels. The optimized H₂ evolution rate reached 577 μmol h^{−1} g^{−1}. This “decorated on 2D” structure is also a promising candidate for direct Z schemes. Dong and coworkers coupled nonmetal plasmonic W₁₈O₄₉ with g-C₃N₄.⁷⁰ The W₁₈O₄₉ nanograsses were assembled on g-C₃N₄ nanosheets by a solvothermal process. This composite showed a photocatalytic response across a very wide spectrum from 450 to 900 nm owing to the dual function of W₁₈O₄₉ as PS II and as hot electron injectors based on the localized SPR (LSPR) effect (Fig. 5). Hence, the H₂ evolution activity was greatly improved and the spectral active range of the photocatalyst was broadened.

In the past few years, hollow structures have been explored widely in photocatalysts because they offer the advantages of enhanced light absorption and more active sites for reaction.⁷² In particular, hollow cubes combine desirable properties such as anisotropic shape⁷³ and specific exposed facets.⁷⁴ Qiu *et al.* firstly designed hollow Co₉S₈ cubes embedded with CdS QDs

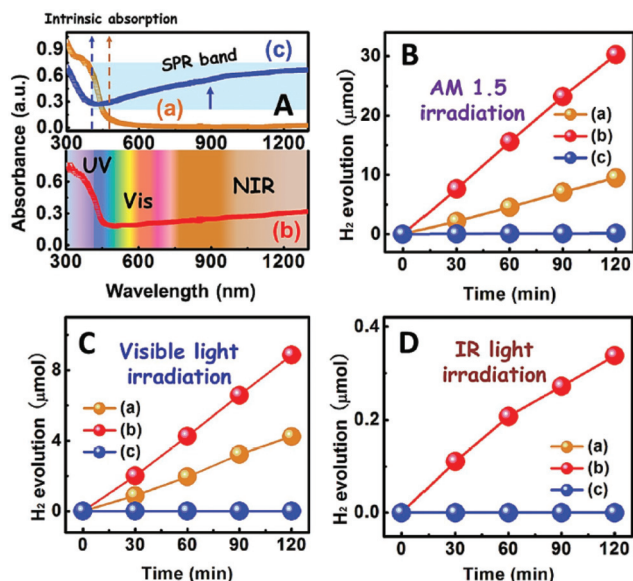


Fig. 5 (A) Light absorption spectra of the as-synthesized samples; photocatalytic performances of the catalysts under (B) AM 1.5G, (C) visible-light, and (D) infrared-light irradiation: (a) $g\text{-C}_3\text{N}_4$, (b) $\text{W}_{18}\text{O}_{49}/g\text{-C}_3\text{N}_4$, and (c) $\text{W}_{18}\text{O}_{49}$ nanograsses. Reproduced from ref. 70 with permission. Copyright 2017 Wiley-VCH Verlag GmbH & Co. KGaA.

as a Z scheme system for photocatalytic water splitting.⁸⁸ The incident light reflected from the $\text{CdS}/\text{Co}_9\text{S}_8$ cubes resulted in improved photocatalytic activity. The hollow $\text{CdS}/\text{Co}_9\text{S}_8$ achieved a much higher H_2 evolution activity (by 134 and 9.1

times) than bare Co_9S_8 and CdS QDs, respectively. This is due to the combined advantages of light harvesting and charge separation by the hollow Z scheme cubes.

To improve the charge flow and surface reaction kinetics, the balance of quantity and size of the two components in a direct Z scheme is a key factor. A “Janus configuration” with comparable sizes and seamless integration of PS I and PS II counterparts may be suitable for direct Z schemes. For example, Yuan *et al.* highlighted a Janus structured $\gamma\text{-MnS}/\text{Cu}_7\text{S}_4$ catalyst with a well defined interface synthesized by cation exchange.⁷⁵ Due to the synergistically improved charge separation and widened light absorption range, the H_2 evolution rates were reported as $718 \mu\text{mol g}^{-1} \text{h}^{-1}$ under UV-Vis irradiation without any noble metal co-catalysts (Fig. 6).

It is worth noting that if the PS I and PS II have similar morphologies they can come into direct contact over enlarged interfaces, especially in 2D/2D heterojunctions. Through rational control of the energy band alignment of the two semiconductors, a 2D/2D direct Z scheme can thus be formed.^{76–81} Theoretical calculations have verified that some 2D van der Waals nanostructures can be integrated into direct Z schemes and applied in photocatalytic water splitting.^{82–84} Zhu *et al.* constructed a 2D/2D heterojunction using narrow-bandgap black phosphorus (BP) and BiVO_4 as PS I and PS II, respectively.⁸⁵ The staggered alignment of band structures allowed Z schematic photolysis of pure water into H_2 ($160 \mu\text{mol g}^{-1} \text{h}^{-1}$) and O_2 ($102 \mu\text{mol g}^{-1} \text{h}^{-1}$) under visible light (Fig. 7). In a subsequent study, BP was further coupled with Bi_2WO_6 monolayers.⁸⁶ The formed heterojunctions showed high photo-

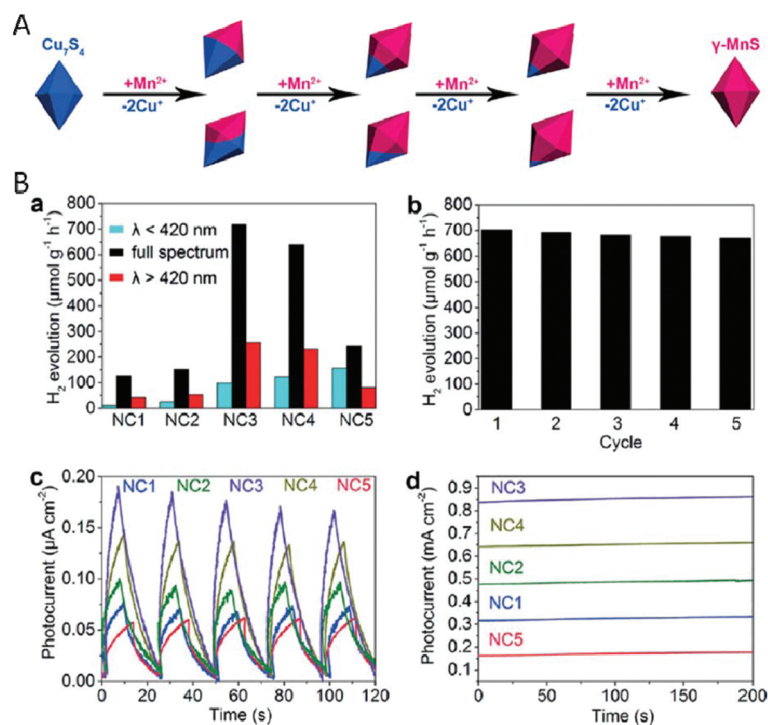


Fig. 6 (A) Schematic illustration of the cation exchange evolution by precisely controlling the reaction time. (B) Photocatalytic and PEC measurements. Reproduced from ref. 75 with permission. Copyright 2017 Wiley-VCH Verlag GmbH & Co. KGaA.

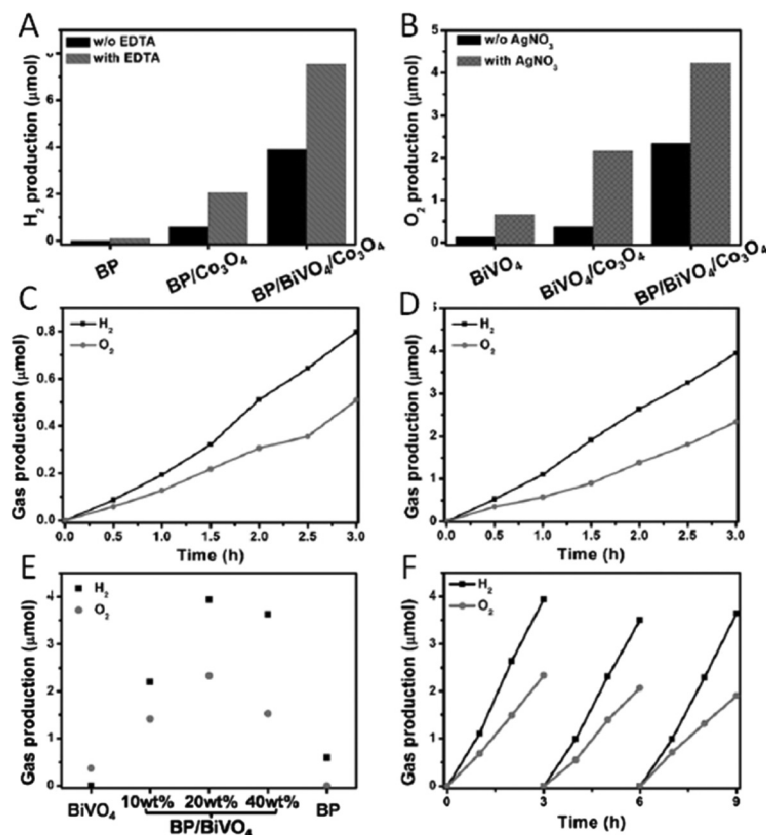


Fig. 7 Photocatalytic production of (A) H_2 and (B) O_2 from water with and without scavengers. Photocatalytic pure water splitting with (C) BP/BiVO₄ and (D) BP/BiVO₄/Co₃O₄. (E) Effect of BP content on photocatalytic water splitting. (F) Stability of BP/BiVO₄/Co₃O₄ photocatalyst. Reproduced from ref. 85 with permission. Copyright 2018 Wiley-VCH Verlag GmbH & Co. KGaA.

Table 1 Representative all-solid-state Z scheme photocatalysts for water splitting

PS I	PS II	Mediator	Activity ($\mu\text{mol h}^{-1} \text{g}^{-1}$, otherwise specified)	Apparent quantum yield (%)	Ref.
SrTiO ₃ :Rh	Au/TiO ₂	Au	H_2 : 5.6, O_2 : 2.7		30
g-C ₃ N ₄	C-TiO ₂	Au	H_2 : 129.0		31
ZnRh ₂ O ₄	Ag _{1-x} SbO _{3-y}	Ag	H_2 : 0.017	0.04 (420 nm)	25
SrTiO ₃ :La/Rh	Ir/CoO _x /Ta ₃ N ₅	Ir	H_2 : 280, O_2 : 140	1.1 (420 nm)	37
PbBi ₂ Nb _{1.5} Ti _{0.109}	WO ₃	W	H_2 : 49.3, O_2 : 741		39
Ru/SrTiO ₃ :Rh	BiVO ₄	RGO	H_2 : 11, O_2 : 5.5	1.03 (420 nm)	19
CeVO ₄	BiVO ₄	3D RGO	O_2 : 85.68		41
g-C ₃ N ₄	Cd _{0.5} Zn _{0.5} S	RGO	H_2 : 39.24×10^3	37.88 (420 nm)	43
Pt/CuGaS ₂	CoO _x /BiVO ₄	RGO	H_2 : 3.5, O_2 : 1.7		47
Pt/CuGaS ₂	TiO ₂	RGO	H_2 : 19.8, O_2 : 10.3	1.3 (380 nm)	48
CdS	BiVO ₄	CDs	H_2 : 1.24, O_2 : 0.61		44
NiO	BiVO ₄	CDs	H_2 : 1.21, O_2 : 0.60		45
La ₅ Ti ₂ Cu _{0.9} Ag _{0.1} S ₅ O ₇	BiVO ₄	Au layer	STH = 0.11%	4.9 (420 nm)	23
SrTiO ₃ :La,Rh	BiVO ₄ :Mo	Au layer	STH = 1.1% (288 K, 5 kPa)	33 (419 nm)	32
RhCrO _x /LaMg _{1/3} Ta _{2/3} O ₂ N	BiVO ₄ :Mo	Au layer	STH = 0.001%	0.07 (418 nm)	36
SrTiO ₃ :La,Rh	BiVO ₄	Au layer	STH = 0.2%	5.9 (418 nm)	56
Ru/SrTiO ₃ :La,Rh	BiVO ₄ :Mo	Carbon	STH = 1.0% (331 K, 91 kPa)	26 (419 nm)	40
SrTiO ₃ :La,Rh	BiVO ₄	np-ITO	STH = 0.4% (331 K, 91 kPa)	10.2 (420 nm)	59
g-C ₃ N ₄	CdS	None	H_2 : $14.9 \mu\text{mol h}^{-1}$	3.8 (420 nm)	62
g-C ₃ N ₄	WO ₃	None	H_2 : 3.12×10^3		63
g-C ₃ N ₄	CoTiO ₃	None	H_2 : 858	38.4 (365 nm)	64
ZnIn ₂ Se ₄	In ₂ O ₃	None	H_2 : 6.95×10^3		65
BCN	TiO ₂	None	H_2 : $3.01 \mu\text{mol h}^{-1}$		67
g-C ₃ N ₄	MnO ₂	None	H_2 : 28.0×10^3	23.33 (420 nm)	68
DR-CNNS	DR-TiO ₂	None	H_2 : 651.8, O_2 : 419.3 $\mu\text{mol h}^{-1}$		69
g-C ₃ N ₄	W ₁₈ O ₄₉	None	H_2 : $15.2 \mu\text{mol h}^{-1}$		70
MoS ₂	g-C ₃ N ₄	None	H_2 : 577		71
Cu ₇ S ₄	MnS	None	H_2 : 718		75
Black phosphorus	BiVO ₄	None	H_2 : 160, O_2 : 102	0.89 (420 nm)	85
Aza-fused microporous polymers	C ₂ N	None	STH = 0.23%	4.3 (600 nm)	87
Co ₉ S ₈	CdS	None	H_2 : 1061.3		88

catalytic activity in H₂ evolution owing to the intimate contact between BP and the Bi₂WO₆ thin layers. Due to the Z schematic mechanism, the CB of BP and VB of Bi₂WO₆ were both strong enough to generate superoxide anion free radicals and holes for efficient nitrogen oxide degradation. Wang *et al.* formed metal-free Z scheme photocatalysts by integrating azafused microporous polymers and C₂N into van der Waals heterostructures.⁸⁷ In this direct Z scheme, the density of photoinduced excitons was enhanced and their lifetime was prolonged. As a result, it achieved an STH efficiency of 0.23% with a rate ratio of 2 : 1 for the photocatalytic H₂ and O₂ evolution. Additionally, the STH further reached 0.40% in a 2D/2D/2D system with RGO acting as a solid mediator. The recent research outcomes in all-solid-state Z scheme systems for photocatalytic water splitting are summarized in Table 1.

4. Conclusions and perspective

Over the past two decades, a tremendous amount of research results have been reported on Z scheme water splitting aiming to achieve practicable photosynthesis on an “artificial leaf”. To date, this goal still remains challenging. The AQE and STH of photocatalytic water splitting by Z scheme systems are still far from satisfactory due to the complex mechanism along with non-negligible competitive reactions. Efficient connection and matching between the two photosystems is the key to improve the photocatalytic activity. We anticipate that the combination of experimental and theoretical studies will further provide in-depth understanding of the structure–function relationship of Z scheme photocatalysts and their applications. More profound insights need to be obtained on the surface kinetics of charge transport between the photosystems and on the water splitting reactions.

Moreover, compared to single photocatalysts, Z scheme systems have the advantage of a wider choice of materials due to the less strict requirement for the bandgaps of PS I and II. Nevertheless, most developed Z schemes still use ultraviolet or visible light responsive materials (*e.g.*, TiO₂, BiVO₄, CdS, g-C₃N₄, WO₃) as building blocks. The infrared part of the solar spectrum is still rarely utilized in Z schematic water photolysis. The development of narrow-bandgap materials (<1.8 eV) with superior quantum efficiency and suppressed carrier recombination is still a need. Furthermore, the development of low-bandgap materials could also promote the full usage of the solar spectrum by forming tandem photocatalytic systems which absorb complementary wavelengths on each photocatalyst. In order to construct Z schematic systems with extended light absorption, especially in the range of infrared light, the PS I and PS II should be made from materials with wider absorption, such as low-bandgap materials (WO₂,⁹² WS₂, black phosphorus, *etc.*), doped semiconductors with intermediate energy levels, and SPR effect materials (Au, W₁₈O₄₉, Cu₂S, *etc.*). In the past years, serious electron–hole recombination in wide absorption materials has limited the development of high performance near-infrared (NIR) photocatalysts. As an

alternative to rational design and finely controlled synthesis to achieve reduced carrier recombination by partnering two long-wavelength-absorption photosystems, another promising strategy may be using upconversion materials (*e.g.*, carbon dots and rare earth metals) and small molecule dyes as antennas to assist the utilization of NIR light.

Finally, due to the difficulty of matching semiconductors with appropriate band structures and surface reaction kinetics, the majority of reported Z schemes could not reach “overall water splitting” but only one half-reaction with the help of scavengers. In this regard, instead of using sacrificial reagents as a flat cost, it would be a better choice to broaden the applied range of new photocatalysts by integrating one half-reaction of water splitting with another significant reaction for clean energy conversion, including: oxygen reduction reaction (ORR), methanol oxidation reaction (MOR), CO₂ reduction reaction (CO₂RR), and nitrogen reduction reaction (NRR). These coupled reactions would be conducive to fully harvesting the potential of solar energy, and many such co-catalysts have been reported. With the great potential and development prospects of photoinduced Z schematic water splitting, artificial photosynthesis with high STH efficiencies will be realized in the near future.

Conflicts of interest

There are no conflicts to declare.

Acknowledgements

This work was supported by National Natural Science Foundation of China (21301110), the Natural Science Foundation of Shandong Province of China (ZR2013BQ011), the Scholarship Fund for Outstanding Young Teachers provided by the Department of Education of Shandong Provincial Government, and the LA BORSF professorship.

References

- 1 T. Hisatomi, J. Kubota and K. Domen, *Chem. Soc. Rev.*, 2014, **43**, 7520–7535.
- 2 A. Kudo and Y. Miseki, *Chem. Soc. Rev.*, 2009, **38**, 253–278.
- 3 A. Fujishima and K. Honda, *Nature*, 1972, **238**, 37–38.
- 4 K. Maeda and K. Domen, *J. Phys. Chem. C*, 2007, **111**, 7851–7861.
- 5 J. Tian, Y. Sang, G. Yu, H. Jiang, X. Mu and H. Liu, *Adv. Mater.*, 2013, **25**, 5074–5074.
- 6 K. Maeda, T. Takata, M. Hara, N. Saito, Y. Inoue, H. Kobayashi and K. Domen, *J. Am. Chem. Soc.*, 2005, **127**, 8286–8287.
- 7 J. Sato, N. Saito, Y. Yamada, K. Maeda, T. Takata, J. N. Kondo, M. Hara, H. Kobayashi, K. Domen and Y. Inoue, *J. Am. Chem. Soc.*, 2005, **127**, 4150–4151.

- 8 G. Zhang, Z.-A. Lan, L. Lin, S. Lin and X. Wang, *Chem. Sci.*, 2016, **7**, 3062–3066.
- 9 Y. Tachibana, L. Vayssieres and J. R. Durrant, *Nat. Photonics*, 2012, **6**, 511.
- 10 K. Sayama, R. Yoshida, H. Kusama, K. Okabe, Y. Abe and H. Arakawa, *Chem. Phys. Lett.*, 1997, **277**, 387–391.
- 11 X. Wang, G. Liu, Z.-G. Chen, F. Li, L. Wang, G. Q. Lu and H.-M. Cheng, *Chem. Commun.*, 2009, 3452–3454, DOI: 10.1039/B904668B.
- 12 X. Wang, G. Liu, L. Wang, Z.-G. Chen, G. Q. Lu and H.-M. Cheng, *Adv. Energy Mater.*, 2012, **2**, 42–46.
- 13 M. C. Hanna and A. J. Nozik, *J. Appl. Phys.*, 2006, **100**, 074510.
- 14 Y. Sasaki, H. Nemoto, K. Saito and A. Kudo, *J. Phys. Chem. C*, 2009, **113**, 17536–17542.
- 15 K. Maeda, M. Higashi, D. Lu, R. Abe and K. Domen, *J. Am. Chem. Soc.*, 2010, **132**, 5858–5868.
- 16 Y. Sasaki, H. Kato and A. Kudo, *J. Am. Chem. Soc.*, 2013, **135**, 5441–5449.
- 17 K. Maeda, D. Lu and K. Domen, *ACS Catal.*, 2013, **3**, 1026–1033.
- 18 S. Chen, Y. Qi, T. Hisatomi, Q. Ding, T. Asai, Z. Li, S. S. K. Ma, F. Zhang, K. Domen and C. Li, *Angew. Chem., Int. Ed.*, 2015, **54**, 8498–8501.
- 19 A. Iwase, Y. H. Ng, Y. Ishiguro, A. Kudo and R. Amal, *J. Am. Chem. Soc.*, 2011, **133**, 11054–11057.
- 20 H. Masanobu, A. Ryu, I. Akio, T. Tsuyoshi, O. Bunsho and D. Kazunari, *Chem. Lett.*, 2008, **37**, 138–139.
- 21 A. Kudo, *MRS Bull.*, 2011, **36**, 32–38.
- 22 H. Li, H. Yu, X. Quan, S. Chen and Y. Zhang, *ACS Appl. Mater. Interfaces*, 2016, **8**, 2111–2119.
- 23 S. Sun, T. Hisatomi, Q. Wang, S. Chen, G. Ma, J. Liu, S. Nandy, T. Minegishi, M. Katayama and K. Domen, *ACS Catal.*, 2018, **8**, 1690–1696.
- 24 H. J. Yun, H. Lee, N. D. Kim, D. M. Lee, S. Yu and J. Yi, *ACS Nano*, 2011, **5**, 4084–4090.
- 25 R. Kobayashi, S. Tanigawa, T. Takashima, B. Ohtani and H. Irie, *J. Phys. Chem. C*, 2014, **118**, 22450–22456.
- 26 L. Ding, H. Zhou, S. Lou, J. Ding, D. Zhang, H. Zhu and T. Fan, *Int. J. Hydrogen Energy*, 2013, **38**, 8244–8253.
- 27 N. Zhang, S. Xie, B. Weng and Y.-J. Xu, *J. Mater. Chem. A*, 2016, **4**, 18804–18814.
- 28 H. Tada, T. Mitsui, T. Kiyonaga, T. Akita and K. Tanaka, *Nat. Mater.*, 2006, **5**, 782.
- 29 Z. B. Yu, Y. P. Xie, G. Liu, G. Q. Lu, X. L. Ma and H.-M. Cheng, *J. Mater. Chem. A*, 2013, **1**, 2773–2776.
- 30 S. Wang, Y. Gao, Y. Qi, A. Li, F. Fan and C. Li, *J. Catal.*, 2017, **354**, 250–257.
- 31 Y. Zou, J.-W. Shi, D. Ma, Z. Fan, C. Niu and L. Wang, *ChemCatChem*, 2017, **9**, 3752–3761.
- 32 Q. Wang, T. Hisatomi, Q. Jia, H. Tokudome, M. Zhong, C. Wang, Z. Pan, T. Takata, M. Nakabayashi, N. Shibata, Y. Li, I. D. Sharp, A. Kudo, T. Yamada and K. Domen, *Nat. Mater.*, 2016, **15**, 611.
- 33 M. Yoshida, K. Takanabe, K. Maeda, A. Ishikawa, J. Kubota, Y. Sakata, Y. Ikezawa and K. Domen, *J. Phys. Chem. C*, 2009, **113**, 10151–10157.
- 34 T. Takata, C. Pan, M. Nakabayashi, N. Shibata and K. Domen, *J. Am. Chem. Soc.*, 2015, **137**, 9627–9634.
- 35 C. Pan, T. Takata, M. Nakabayashi, T. Matsumoto, N. Shibata, Y. Ikumura and K. Domen, *Angew. Chem., Int. Ed.*, 2015, **54**, 2955–2959.
- 36 Z. Pan, T. Hisatomi, Q. Wang, M. Nakabayashi, N. Shibata, C. Pan, T. Takata and K. Domen, *Appl. Catal., A*, 2016, **521**, 26–33.
- 37 Q. Wang, T. Hisatomi, S. S. K. Ma, Y. Li and K. Domen, *Chem. Mater.*, 2014, **26**, 4144–4150.
- 38 Z. Liu, Z.-G. Zhao and M. Miyauchi, *J. Phys. Chem. C*, 2009, **113**, 17132–17137.
- 39 H. G. Kim, E. D. Jeong, P. H. Borse, S. Jeon, K. Yong, J. S. Lee, W. Li and S. H. Oh, *Appl. Phys. Lett.*, 2006, **89**, 064103.
- 40 Q. Wang, T. Hisatomi, Y. Suzuki, Z. Pan, J. Seo, M. Katayama, T. Minegishi, H. Nishiyama, T. Takata, K. Seki, A. Kudo, T. Yamada and K. Domen, *J. Am. Chem. Soc.*, 2017, **139**, 1675–1683.
- 41 Q. Liu, J. Shen, X. Yang, T. Zhang and H. Tang, *Appl. Catal., B*, 2018, **232**, 562–573.
- 42 N. Shehzad, M. Tahir, K. Johari, T. Murugesan and M. Hussain, *Appl. Surf. Sci.*, 2019, **463**, 445–455.
- 43 W. Xue, X. Hu, E. Liu and J. Fan, *Appl. Surf. Sci.*, 2018, **447**, 783–794.
- 44 X. Wu, J. Zhao, L. Wang, M. Han, M. Zhang, H. Wang, H. Huang, Y. Liu and Z. Kang, *Appl. Catal., B*, 2017, **206**, 501–509.
- 45 C. A. Liu, Y. Fu, J. Zhao, H. Wang, H. Huang, Y. Liu, Y. Dou, M. Shao and Z. Kang, *Chem. Eng. J.*, 2019, **358**, 134–142.
- 46 K. S. Novoselov, A. K. Geim, S. V. Morozov, D. Jiang, Y. Zhang, S. V. Dubonos, I. V. Grigorieva and A. A. Firsov, *Science*, 2004, **306**, 666–669.
- 47 A. Iwase, S. Yoshino, T. Takayama, Y. H. Ng, R. Amal and A. Kudo, *J. Am. Chem. Soc.*, 2016, **138**, 10260–10264.
- 48 K. Iwashina, A. Iwase, Y. H. Ng, R. Amal and A. Kudo, *J. Am. Chem. Soc.*, 2015, **137**, 604–607.
- 49 H. Li, Z. Kang, Y. Liu and S.-T. Lee, *J. Mater. Chem.*, 2012, **22**, 24230–24253.
- 50 H. Zhang, H. Ming, S. Lian, H. Huang, H. Li, L. Zhang, Y. Liu, Z. Kang and S.-T. Lee, *Dalton Trans.*, 2011, **40**, 10822–10825.
- 51 Z. Ma, H. Ming, H. Huang, Y. Liu and Z. Kang, *New J. Chem.*, 2012, **36**, 861–864.
- 52 B. C. M. Martindale, G. A. M. Hutton, C. A. Caputo and E. Reisner, *J. Am. Chem. Soc.*, 2015, **137**, 6018–6025.
- 53 X. Wang, L. Cao, F. Lu, M. J. Mezziani, H. Li, G. Qi, B. Zhou, B. A. Harruff, F. Kermarrec and Y.-P. Sun, *Chem. Commun.*, 2009, 3774–3776, DOI: 10.1039/B906252A.
- 54 X. Xia, N. Deng, G. Cui, J. Xie, X. Shi, Y. Zhao, Q. Wang, W. Wang and B. Tang, *Chem. Commun.*, 2015, **51**, 10899–10902.
- 55 T. Minegishi, N. Nishimura, J. Kubota and K. Domen, *Chem. Sci.*, 2013, **4**, 1120–1124.
- 56 Q. Wang, Y. Li, T. Hisatomi, M. Nakabayashi, N. Shibata, J. Kubota and K. Domen, *J. Catal.*, 2015, **328**, 308–315.

- 57 M. Shiraishi and M. Ata, *Carbon*, 2001, **39**, 1913–1917.
- 58 H. B. Michaelson, *J. Appl. Phys.*, 1977, **48**, 4729–4733.
- 59 Q. Wang, S. Okunaka, H. Tokudome, T. Hisatomi, M. Nakabayashi, N. Shibata, T. Yamada and K. Domen, *Joule*, 2018, **2**, 2667–2680.
- 60 Q. Jia, A. Iwase and A. Kudo, *Chem. Sci.*, 2014, **5**, 1513–1519.
- 61 J. Wan, X. Du, E. Liu, Y. Hu, J. Fan and X. Hu, *J. Catal.*, 2017, **345**, 281–294.
- 62 W. Jiang, X. Zong, L. An, S. Hua, X. Miao, S. Luan, Y. Wen, F. F. Tao and Z. Sun, *ACS Catal.*, 2018, **8**, 2209–2217.
- 63 W. Yu, J. Chen, T. Shang, L. Chen, L. Gu and T. Peng, *Appl. Catal., B*, 2017, **219**, 693–704.
- 64 R. Ye, H. Fang, Y.-Z. Zheng, N. Li, Y. Wang and X. Tao, *ACS Appl. Mater. Interfaces*, 2016, **8**, 13879–13889.
- 65 Y. Chao, P. Zhou, N. Li, J. Lai, Y. Yang, Y. Zhang, Y. Tang, W. Yang, Y. Du, D. Su, Y. Tan and S. Guo, *Adv. Mater.*, 2018, 1807226.
- 66 S. Bai, J. Jiang, Q. Zhang and Y. Xiong, *Chem. Soc. Rev.*, 2015, **44**, 2893–2939.
- 67 X. Xing, H. Zhu, M. Zhang, L. Hou, Q. Li and J. Yang, *Catal. Sci. Technol.*, 2018, **8**, 3629–3637.
- 68 Z. Mo, H. Xu, Z. Chen, X. She, Y. Song, J. Lian, X. Zhu, P. Yan, Y. Lei, S. Yuan and H. Li, *Appl. Catal., B*, 2019, **241**, 452–460.
- 69 H. Gao, R. Cao, X. Xu, S. Zhang, H. Yongshun, H. Yang, X. Deng and J. Li, *Appl. Catal., B*, 2019, **245**, 399–409.
- 70 Z. Zhang, J. Huang, Y. Fang, M. Zhang, K. Liu and B. Dong, *Adv. Mater.*, 2017, **29**, 1606688.
- 71 Y. Liu, H. Zhang, J. Ke, J. Zhang, W. Tian, X. Xu, X. Duan, H. Sun, M. O. Tade and S. Wang, *Appl. Catal., B*, 2018, **228**, 64–74.
- 72 X. Wang, J. Feng, Y. Bai, Q. Zhang and Y. Yin, *Chem. Rev.*, 2016, **116**, 10983–11060.
- 73 K. Kato, F. Dang, K.-I. Mimura, Y. Kinemuchi, H. Imai, S. Wada, M. Osada, H. Haneda and M. Kuwabara, *Adv. Powder Technol.*, 2014, **25**, 1401–1414.
- 74 J. Zheng, W. Zhou, Y. Ma, W. Cao, C. Wang and L. Guo, *Chem. Commun.*, 2015, **51**, 12863–12866.
- 75 Q. Yuan, D. Liu, N. Zhang, W. Ye, H. Ju, L. Shi, R. Long, J. Zhu and Y. Xiong, *Angew. Chem., Int. Ed.*, 2017, **56**, 4206–4210.
- 76 W. Chen, Z.-C. He, G.-B. Huang, C.-L. Wu, W.-F. Chen and X.-H. Liu, *Chem. Eng. J.*, 2019, **359**, 244–253.
- 77 Q. Xu, B. Zhu, C. Jiang, B. Cheng and J. Yu, *Sol. RRL*, 2018, **2**, 1800006.
- 78 X. She, J. Wu, H. Xu, J. Zhong, Y. Wang, Y. Song, K. Nie, Y. Liu, Y. Yang, M.-T. F. Rodrigues, R. Vajtai, J. Lou, D. Du, H. Li and P. M. Ajayan, *Adv. Energy Mater.*, 2017, **7**, 1700025.
- 79 J. Shi, S. Li, F. Wang, Y. Li, L. Gao, X. Zhang and J. Lu, *Catal. Sci. Technol.*, 2018, **8**, 6458–6467.
- 80 J. Fu, Q. Xu, J. Low, C. Jiang and J. Yu, *Appl. Catal., B*, 2019, **243**, 556–565.
- 81 J. Wang, X. Li, Y. You, X. Yang, Y. Wang and Q. Li, *Nanotechnology*, 2018, **29**, 365401.
- 82 L. Ju, Y. Dai, W. Wei, M. Li and B. Huang, *Appl. Surf. Sci.*, 2018, **434**, 365–374.
- 83 C.-F. Fu, Q. Luo, X. Li and J. Yang, *J. Mater. Chem. A*, 2016, **4**, 18892–18898.
- 84 R. Zhang, L. Zhang, Q. Zheng, P. Gao, J. Zhao and J. Yang, *J. Phys. Chem. Lett.*, 2018, **9**, 5419–5424.
- 85 M. Zhu, Z. Sun, M. Fujitsuka and T. Majima, *Angew. Chem., Int. Ed.*, 2018, **57**, 2160–2164.
- 86 J. Hu, D. Chen, Z. Mo, N. Li, Q. Xu, H. Li, J. He, H. Xu and J. Lu, *Angew. Chem.*, 2019, **131**, 2095–2099.
- 87 L. Wang, X. Zheng, L. Chen, Y. Xiong and H. Xu, *Angew. Chem.*, 2018, **130**, 3512–3516.
- 88 B. Qiu, Q. Zhu, M. Du, L. Fan, M. Xing and J. Zhang, *Angew. Chem., Int. Ed.*, 2017, **56**, 2684–2688.
- 89 P. Zhou, J. Yu and M. Jaroniec, *Adv. Mater.*, 2014, **26**, 4920–4935.
- 90 H. Li, W. Tu, Y. Zhou and Z. Zou, *Adv. Sci.*, 2016, **3**, 1500389.
- 91 H. Li, Y. Gao, Y. Zhou, F. Fan, Q. Han, Q. Xu, X. Wang, M. Xiao, C. Li and Z. Zou, *Nano Lett.*, 2016, **16**, 5547–5552.
- 92 G. Cui, W. Wang, M. Ma, J. Xie, X. Shi, N. Deng, J. Xin and B. Tang, *Nano Lett.*, 2015, **15**, 7199–7203.